Contents lists available at GrowingScience

Engineering Solid Mechanics

homepage: www.GrowingScience.com/esm

# Opening-tearing mixed-mode fracture behavior of rock using ENDB, ENDC, DNDC, SCB, TPB-IC, SENB, and ATPB specimens

**A. Mousavi[a], M.R.M. Aliha[b,c*], H. Khoramishad[a*], H. R. Karimi[c], N. Choupani[b] and T. Sadowski[d]**

[a]*Adhesively bonded and sandwich structures research laboratory, School of Mechanical Engineering, Iran University of Science and Technology, Narmak, 16846-13114, Tehran, Iran*
[b]*Department of Mechanical Engineering, Gebze Technical University, Kocaeli, 41400, Turkiye*
[c]*Welding and joining research center, School of Industrial Engineering, Iran University of Science and Technology, Narmak, 16846-13114, Tehran, Iran*
[d]*Department of Solid Mechanics, Lublin University of Technology, Nadbystrzycka 40 Str., 20-216, Lublin, Poland*

**ARTICLEINFO**

*Article history*:
Received 8 June 2024
Accepted 18 December 2024
Available online
18 December 2024

*Keywords*:
*Mixed mode I/III Fracture*
*Rock*
*Different circular and beam shape testing methods*
*Geometry and loading effects*
*Fracture envelopes*

**ABSTRACT**

This paper investigates experimentally and numerically the influence of geometry and loading conditions on the fracture response of rock materials. Seven different test samples namely "Edge-Notched-Disc-Bend (ENDB), Semi-Circular-Bend (SCB), Three-Point-Bend-Inclined-Crack (TPB-IC), Single-Edge-Notched-Bending (SENB), Asymmetric-Three-Point-Bend (ATPB), Edge-Notched-Disc-Compression (ENDC) and Double-Notched-Disc-Compression (DNDC)" made of a marble rock were manufactured and tested under bending and compressive loading conditions. The results showed that the failure loads of all samples increase with the change of pure mode I to pure mode III. However, the corresponding fracture toughness values of ENDB, SCB, TPB-IC, SENB and ATPB specimens decreased, while the ENDC and DNDC samples experienced an increase in the fracture toughness. Among the studied specimens, only the ENDB, ENDC and DNDC samples presented pure mode III with $K_{IIIc}/K_{Ic}$ ratio ranging from 0.735 for the ENDB specimen to 2.076 for the DNDC sample. The highest mode-I fracture toughness among all the studied specimens was obtained for the SENB and TPB-IC samples, with a value of 1.54 MPa $m^{0.5}$, while the lowest value was obtained for the DNDC specimen with a value of 1.21 MPa $m^{0.5}$. The sign and the magnitude of T-stress considerably depended on the loading condition and geometry of the specimens. The crack trajectories of all specimens under study were also investigated.



## 1. Introduction

Defects and cracks can occur in different materials for various reasons. The cracked, brittle materials such as rocks, concretes, ceramics, and polymers are prone to catastrophic failure and fast fracture. Therefore, analyzing the fracture behavior of the cracked components made of brittle materials using the fracture mechanics concepts is critical. A crack can propagate under three fracture modes including opening, sliding (in-plane shear) and tearing (out-of-plane shear). However, cracked components are usually subjected to mixed-mode loading conditions. Fracture toughness is the most essential material parameter in defining the material resistance to fracture. This material parameter is dependent on the cracked specimen and its geometry. Researchers have studied the dependency of the opening-sliding mixed-mode fracture behavior of quasi-brittle materials on the specimen geometry. Several test specimens with different geometries have been employed so far for the investigation of the opening and opening-sliding fracture behaviors of engineering materials (Hoseini et al., 2022,2023,2024). Some of the specimen geometries used for assessing the opening-sliding fracture have disc shape specimen with a chevron notch or central crack (Awaji and Sato, 1978; Ayatollahi & Aliha, 2008; Cao et al., 2023; Zheng et al., 2022). Other samples including the triangular and semicircular samples under 3-point bending (Aliha et al., 2010; Ayatollahi et al., 2011; Guan et al., 2022; Li et al., 2023; Zhang et al., 2014), the edge-cracked rectangular beam subjected to 3- or 4-point bending (Aliha et

* Corresponding author.
E-mail addresses: mrm_aliha@iust.ac.ir (M.R.M. Aliha)

ISSN 2291-8752 (Online) - ISSN 2291-8744 (Print)

doi: 10.5267/j.esm.2024.12.001

al., 2022; Maccagno & Knott, 1989; Xeidakis et al., 1996), the compact tension-shear specimen (Abdollahipour et al., 2016; Hasanpour & Choupani, 2009; Mahajan & Ravi-Chandar, 1989; Qiu et al., 2020; Wan et al., 2022; Yao et al., 2021), and the ring shape specimens (Karimi et al., 2022) are to name a few for spanning the complete range of opening-sliding modes of fracture. Aliha & Ayatollahi, (2010); Aliha et al., (2010), Bazoobandi et al., (2024); Karimi et al., 2024; Shabakhty et al., (2024) compared the mixed-mode I/II fracture behavior of various specimens with different geometries and showed that the geometry of the cracked specimens could considerably affect the mixed-mode I/II fracture behavior

One of the mixed-mode loading conditions is related to the combination of opening and tearing (Bidadi et al., 2022; Sreenath et al., 2022; Gan et al., 2024; Shui et al., 2024; Bahmani & Nemati., 2021). Geomaterials such as rocks may undergo opening-tearing mixed-mode loading in civil and mining operations (Bahmani et al., 2021; Raeisi et al., 2024; Mousavi et al., 2024; Gan et al., 2021; Shi et al., 2024, Liu and Ma., 2023, Yang et al., 2022; Najjar et al., 2022; Cui & McAdie, 2023; Pournoori et al., 2024; Ahmadi et al., 2021; Tang et al., 2024). The tearing fracture response of materials can be studied using a torsional-type loading setup. However, executing a torsional-type load directly on geomaterials such as concretes and rocks is not conveniently implementable for introducing mode-III deformation. Moreover, the application of torsional torque needs special fixtures (Marat-Mendes & DeFreitas, 2009) that may not be available in most test laboratories. Alternatively, out-of-plane shear deformation can be applied to the cracked specimens using indirect testing methods through compression or bending loads that are more accessible in laboratories. Some works and researches such as (Aliha et al., 2015, 2017a,2021; Zhao et al ., 2024; Pirmohammad & Bayat., 2016, Mousavi et al., 2021; Zarei et al., 2021, 2022; Khanghahi et al., 2024) have suggested disc-shaped specimens with edge cracks subjected to bending and diametral compression for conducting opening-tearing fracture experiments on different quasi-brittle materials. The cracked disc-shaped samples in the aforementioned works were: Edge-Notched-Disc-Bend (ENDB) specimen proposed by (Aliha et al., 2015), Edge-Notched-Disc-Compression (ENDC) specimen (Aliha et al., 2017c) and Double-Notched-Disc-Compression (DNDC) sample suggested by (Aliha et al., 2021). These specimens have two main positive points, including (i) their circular shape that facilitates the specimen preparation from rock cores, and (ii) the tearing test can indirectly be applied using the 3-point bending or compression fixtures with universal testing machines. (Pirmohammad & Kiani, 2016) used the SCB specimen made of asphalt with a new configuration to obtain the opening-tearing mixed mode. Pan et al. (Pan et al., 2021) provided a different opening, sliding and tearing combinations using the Three-Point-Bend-Inclined-Crack (TPB-IC) specimen. They obtained pure opening mode and different mixed-mode conditions by varying the crack angle. Ahmadi Moghadam and Taheri (2013) suggested the Single-Edge-Notched-Beam (SENB) specimen and proposed a set of practical equations, by which one could evaluate mixed-mode I/III stress intensity factors. Li et al. (2023) tested the Asymmetric-Three-Point-Bend (ATPB) specimen at different temperatures to investigate the mixed-mode I/III fracture behavior (Li-yun et al., 2013). Pietras and coworkers (Pietras et al., 2021,2023) also utilized cylindrical shape samples containing circumferential notch and subjected to far-field tension and compression to conduct mode I and mode III fracture tests on geomaterials such as gypsum and aerated concrete. Among the available mixed mode I/III test samples, the ENDB specimen has received much attention by the geomaterial and construction and building materials researchers (e.g., Najjar et al., (2020, 2022), Hoseini et al., (2022,2023), Bahmani et al., (2019), Karimi et al., (2023), Bakhshizadeh et al., (2024)). A review of mixed mode fracture tests for different materials and, in particular, those works describing the contribution of mode III or out-of-plane tear deformation, has also been published recently by Aliha and coworkers (Aliha et al., 2023). Although several researchers have studied opening-tearing mixed-mode fracture in brittle materials, there is no comprehensive research to compare the influence of the loading condition and sample geometry on the opening-tearing fracture of brittle materials. This paper investigates the influence of loading conditions and specimen geometry on the fracture behavior of brittle materials by focusing on the specimens that can provide opening-tearing mixed-mode conditions with compression and bending-type loads. Seven geometries, including three disc-shaped samples with different pre-crack positions, one semicircular bending sample and three rectangular samples under 3-point bending, were manufactured from a rock material and tested. The stress intensity factor (SIF) and *T*-stress values were obtained from numerical modelling. Therefore, this work can provide a comprehensive insight into the fracture response of quasi-brittle and brittle materials subjected to opening-tearing mixed-mode loading.

## 2. Materials and specimens

To study the influence of geometry on the fracture response of brittle materials under mixed opening/out-of-plane shear loading, rock material was used. The advantage of this type of rock (Gohareh marble) extracted from the mines of Lorestan (Iran), is its integrity and lack of veins, which makes it suitable for testing in the field of fracture mechanics. Also, the brittleness of this type of rock is a fundamental factor in its selection because the size of the plastic zone in the vicinity of the crack tip is small enough, so the concepts of linear elastic fracture mechanics are applicable (Aliha et al., 2010, 2017a; Aliha & Ayatollahi, 2014). Seven specimens were considered in the current study to investigate the influence of geometry on the fracture of brittle materials under tension-tear loading. Fig. 1 shows the numerical models of the specimens considered in this study, namely ENDB, ENDC, DNDC, SCB, TPB-IC, SENB and ATPB samples. In addition, the geometrical dimensions of the specimens ($R$, $L$, $B$, $t$ and $W$), the loading supports ratio ($S/R$ or $S/L$), and the crack length to thickness ratio ($a/B$ or $a/W$ or $a/R$) are specified in Table 1. According to the geometrical dimensions listed in Table 1, the depth of crack ($a$) for the ENDB and ENDC was taken at 13.2 mm and the depth of crack at each side (i.e., $a/2$) for the double-notched sample (i.e., DNDC) was considered equal to 9.9 mm. For the SCB specimen, the crack depth was 0.4 times the radius with a value of 16.8 mm. The crack depth in the TPB-IC and SENB specimens was considered equal to 12 mm. Finally, for the ATPB specimen, the crack depth was considered equal to 13.2 mm. Pure mode-I loading was obtained when the crack inclination angle (α) was

considered zero in the ENDB, ENDC, DNDC, SCB, TPB-IC, and SENB specimens. By increasing the crack inclination angle from zero, the footprint of tearing mode became available, and the specimens were placed under the condition of opening-tearing mixed-mode. However, in the ATPB specimen, pure opening loading was achieved by considering zero value for $l$ (see Fig. 1(e)) and the opening-tearing mixed-mode loading was accessible by shifting the crack toward the support. To study the geometry effect on the fracture behavior of the ENDB, ENDC, DNDC, SCB, TPB-IC, SENB, and ATPB specimens, it was necessary to determine the SIFs for different geometrical and loading conditions. SIFs of the samples in this study were considered as the functions of the applied load ($P$), the crack length ($a$), the crack inclination angle ($\alpha$), the spacing between the supports ($S$) and can be determined using Eqs. (1-6) (Aliha & Bahmani, 2017; Aliha et al., 2023; Bahmani et al., 2019; Li-yun et al., 2013; Pan et al., 2021; Pirmohammad & Kiani, 2016).

**Table 1.** The values of geometrical parameters for different specimens.

| specimens | $R$ or $L$ (mm) | $B$ or $t$ (mm) | $a/B$ or $a/W$ or $a/R$ | $S/R$ or $S/L$ | $W$(mm) |
|---|---|---|---|---|---|
| ENDB | 47 | 33 | 0.4 | 0.9 | - |
| ENDC | 47 | - | 0.4 | - | 33 |
| DNDC | 47 | - | 0.6 | - | 33 |
| SCB | 42 | 33 | 0.4 | 0.8 | - |
| TPB-IC | 100 | 23 | 0.4 | 0.8 | 30 |
| SENB | 100 | 23 | 0.4 | 0.8 | 30 |
| ATPB | 100 | 33 | 0.4 | 0.8 | 23 |

$$K_{\mathrm{i(ENDB)}} = \frac{3PS}{2RB^2}\sqrt{\pi a}\; Y_{\mathrm{i}}\left({}^{a}/_{B}\,.\,{}^{S}/_{R}\,.\,\alpha\right) \tag{1}$$

$$K_{\mathrm{i(ENDC)}} = \frac{P}{RB}\sqrt{\pi a}\; Y_{\mathrm{i}}\left({}^{a}/_{B}\,.\,\alpha\right) \tag{2}$$

$$K_{\mathrm{i(DNDC)}} = \frac{P}{RB}\sqrt{\pi\frac{a}{2}}\; Y_{\mathrm{i}}\left({}^{a}/_{B}\,.\,\alpha\right) \tag{3}$$

$$K_{\mathrm{i(SCB)}} = \frac{P}{2Rt}\sqrt{\pi a}\; Y_{\mathrm{i}}\left({}^{a}/_{R}\,.\,{}^{S}/_{R}\,.\,\alpha\right) \tag{4}$$

$$K_{\mathrm{i(TPB-IC\ and\ SENB)}} = \frac{PS}{BW^2}\sqrt{\pi a}\; Y_{\mathrm{i}}\left({}^{a}/_{W}\,.\,\alpha\right) \tag{5}$$

$$K_{\mathrm{i(ATPB)}} = \frac{PS}{WB^2}\sqrt{\pi a}\; Y_{\mathrm{i}}\left({}^{a}/_{W}\,.\,\alpha\right) \tag{6}$$

where $Y_{\mathrm{i}}$ (i = I, II, III) represent the geometry factors of the mentioned specimens and are considered as the functions of $a/B$, $S/R$, and $\alpha$. These geometry factors are non-dimensional forms of the SIFs ($K_{\mathrm{I}}$, $K_{\mathrm{II}}$, and $K_{\mathrm{III}}$). The geometry factors can be obtained using numerical finite element modeling.

## 3. Numerical analysis

The ENDB, ENDC, DNDC, SCB, TPB-IC, SENB, and ATPB specimens were modelled with the ABAQUS finite element code to obtain the fracture parameters (i.e. SIF and $T$-stress values). The specifications and dimensions of all samples are shown in Table 1. Fig. 1 shows the finite element models of different specimens. The elastic modulus and the Poisson's ratio of the tested marble (Gohareh rock) were considered as 35 GPa and 0.25 (Aliha & Bahmani, 2017), respectively.

The twenty-node quadratic brick elements were used to model the specimens. The total numbers of elements used for modelling different specimens were approximately 54000, 56000, 64000, 31000, 27000, 27000, and 28000 for the ENDB, ENDC, DNDC, SCB, TPB-IC, SENB, and ATPB samples, respectively. For modelling the singularity of the stress field, singular elements were employed in the first element row around the crack tip and across the crack front, as shown in **Fig. 1.** The failure loads obtained from the tests of the specimens were used in finite element modelling. **Fig. 2** depicts the variations of opening and tearing mode geometry factors ($Y_{\mathrm{I}}$ and $Y_{\mathrm{III}}$) obtained at the central portion of the ENDB, ENDC, DNDC, SCB, TPB-IC and SENB samples for different crack inclination angles and at the mid-section of the ATPB specimen for different distances from the center.

Fig. 2 shows that increasing the angle of crack inclination in the ENDB, ENDC, DNDC, SCB, TPB-IC and SENB samples decreased the opening-mode geometry factor ($Y_{\mathrm{I}}$) and, conversely, increased the tearing-mode geometry factor ($Y_{\mathrm{III}}$). Similarly, increasing the $l$ distance in the ATPB specimen decreased the opening-mode geometry factor ($Y_{\mathrm{I}}$) and increased the tearing-mode geometry factor ($Y_{\mathrm{III}}$). In addition to SIF, the $T$-stress (the first nonsingular stress term in the Williams series) can considerably influence the mixed-mode fracture responses and behaviors of the specimens. From the numerical results, the maximum $T$-stress value along the crack front was obtained at the mid-point of the crack front for different specimens of this research. Hence, this value was reported as the magnitude of $T$-stress in the present study. It is important to mention that the ABAQUS finite element code uses the interaction J-integral method to determine the $T$-stress (Gao et al., 2023; Toshio & Parks, 1992; Yu & Kuna, 2021).

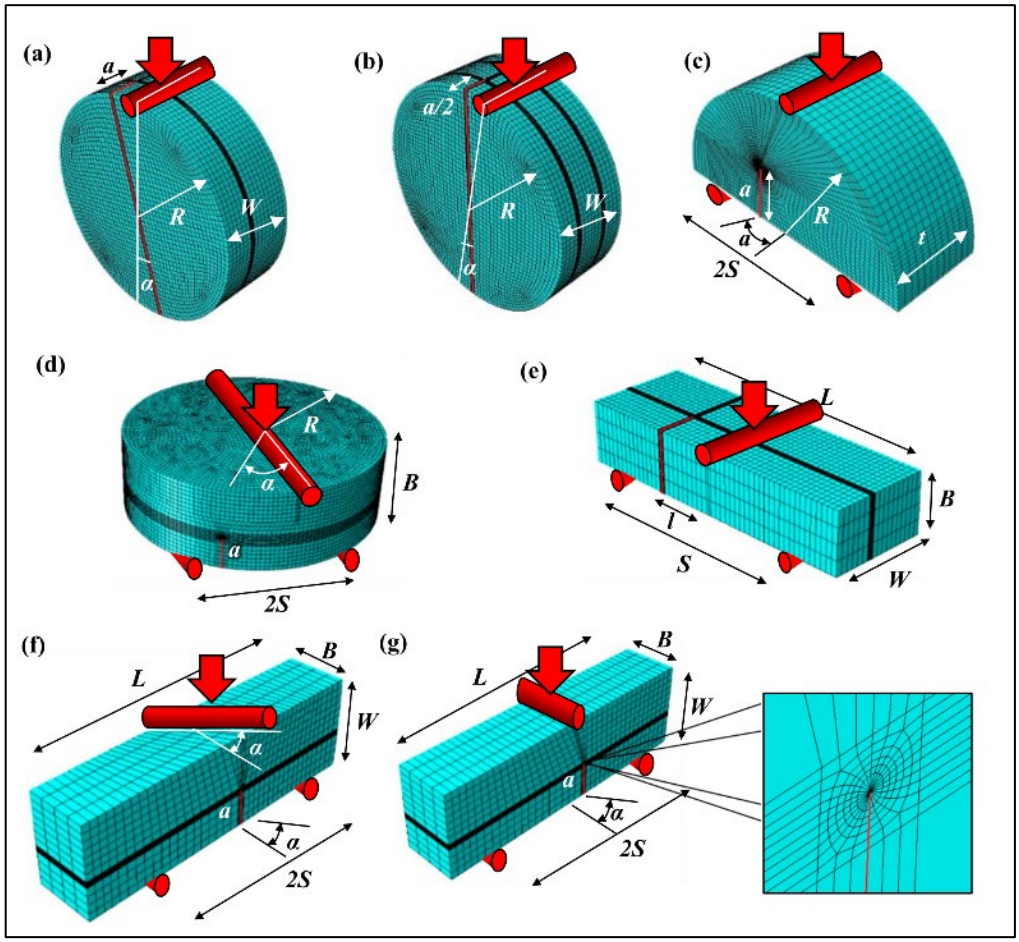


**Fig. 1.** Finite element models of different specimens; (a) ENDC, (b) DNDC, (c) SCB, (d) ENDB, (e) ATPB, (f) SENB, and (g)TPB-IC

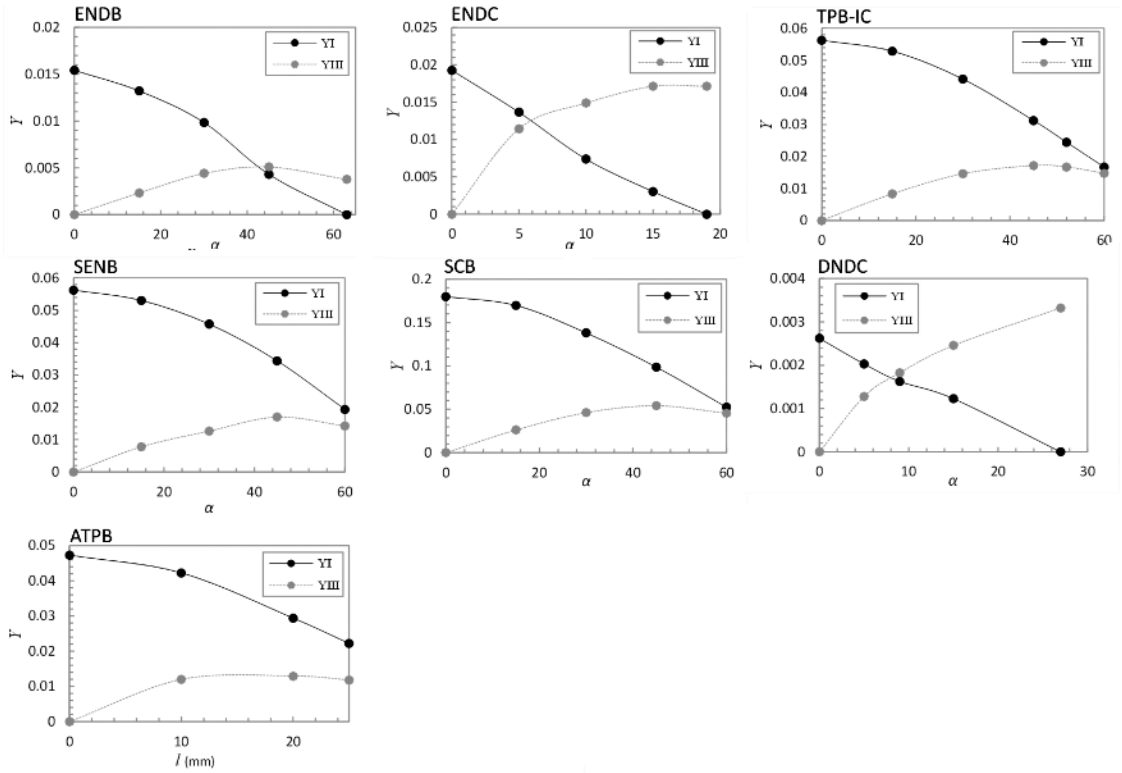


**Fig. 2.** The geometry factors as a function of $\alpha$ for the ENDB, ENDC, DNDC, SCB, TPB-IC, SENB, and ATPB specimens and as a function of $l$ for the ATPB specimen.

**Fig. 3** depicts the variations of $T$-stress value in terms of $M_e^{13}$ for different specimens. $M_e^{13}$ is the mode mixity parameter defined in Eq. (7).

$$M_e^{13} = \frac{2}{\pi}\tan^{-1}\left(\frac{K_I}{K_{III}}\right) \tag{7}$$

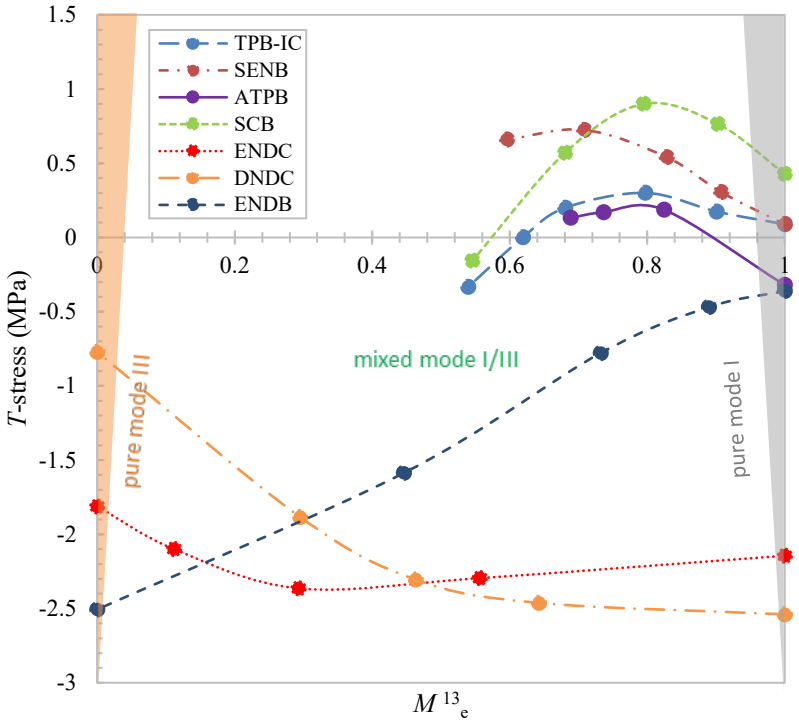


**Fig. 3.** Variations of $T$-stress for different mode mixities at the mid-points of different specimens.

As can be seen in **Fig. 3**, the $T$-stress values obtained for different geometries and loading conditions were different, even though the mode mixity and the material were the same. Therefore, the sign and the magnitude of $T$-stress obtained for different specimens were found to be considerably dependent on the geometry and loading conditions of the specimens. This is important, as $T$-stress can considerably affect the accuracy of the fracture toughness and crack growth path estimations (Ayatollahi et al., 1998; Fan et al., 2021; Smith et al., 2001; Smith et al., 2006, Mirsayar et al., 2014). According to Fig. 3, in pure mode I ($M_e^{13} = 1$), the highest positive $T$-stress value was obtained for the SCB specimen, while the highest negative $T$-stress value was obtained for the DNDC specimen. Among the specimens studied in this research, only three specimens could cover pure mode III including the DNDC, ENDC and ENDB for which the $T$-stress value was negative throughout the full band of mode mixity. In pure mode III, the highest negative value of $T$-stress was obtained for the ENDB sample, while the lowest negative value of $T$-stress was attained for the DNDC sample.

The critical SIF values are commonly taken as the material fracture toughness ($K_{Ic}$ and $K_{IIIc}$). However, if the $T$-stress value is negligible, the stress intensity factor critical value can be directly corresponded to the critical stress component close the crack tip and can be considered as a material property (Ayatollahi et al., 1998; Smith et al., 2001; Smith et al., 2006). Otherwise, the positive or negative values of $T$-stress can influence the SIF critical value and increase or decrease the apparent fracture toughness value, respectively (Aliha et al., 2017a,d; Ayatollahi & Saboori, 2015; Smith et al., 2001). According to Fig. 3, the values of fracture toughness determined from the TPB-IC, SENB, SCB, ENDB and ATPB specimens under pure mode-I loading can be relatively reliable, because the magnitude of $T$-stress for these specimens was negligible at pure opening mode and therefore, the fracture toughness was independent of the test specimen geometry and loading conditions.

## 4. Fracture toughness experiments

In this research, seven different test configurations and specimens with the dimensions specified in Table 1 were cut from Gohareh rock to study the influence of geometry on the opening-tearing mixed-mode fracture of rocks. A saw blade was employed to produce pre-cracks in the specimens. For each experiment, different ratios of mixed mode from pure opening mode to the opening-tearing mixed mode and pure tearing mode were considered to perform the fracture toughness tests. The considered inclination angles of crack and the related values of the geometry factors are listed in Table 2. At least three replicates were considered for each test case to ensure the repeatability of the experimental results.

**Table 2.** Specifications of the opening-tearing mixed-mode test samples and the geometry factor values

| Specimens | Geometry factors ($Y_I$ and $Y_{III}$) | | | | | | | | | |
|---|---|---|---|---|---|---|---|---|---|---|
| ENDB | $\alpha = 0^\circ$ | | $\alpha = 15^\circ$ | | $\alpha = 30^\circ$ | | $\alpha = 45^\circ$ | | $\alpha = 63^\circ$ | |
| | $Y_I$ | $Y_{III}$ | $Y_I$ | $Y_{III}$ | $Y_I$ | $Y_{III}$ | $Y_I$ | $Y_{III}$ | $Y_I$ | $Y_{III}$ |
| | 0.01541 | 0 | 0.01321 | 0.00232 | 0.00984 | 0.00441 | 0.00429 | 0.00510 | 0 | 0.00377 |
| ENDC | $\alpha = 0^\circ$ | | $\alpha = 5^\circ$ | | $\alpha = 10^\circ$ | | $\alpha = 15^\circ$ | | $\alpha = 19^\circ$ | |
| | $Y_I$ | $Y_{III}$ | $Y_I$ | $Y_{III}$ | $Y_I$ | $Y_{III}$ | $Y_I$ | $Y_{III}$ | $Y_I$ | $Y_{III}$ |
| | 0.01927 | 0 | 0.01366 | 0.01144 | 0.00738 | 0.01489 | 0.00303 | 0.01713 | 0 | 0.01714 |
| DNDC | $\alpha = 0^\circ$ | | $\alpha = 5^\circ$ | | $\alpha = 9^\circ$ | | $\alpha = 15^\circ$ | | $\alpha = 27^\circ$ | |
| | $Y_I$ | $Y_{III}$ | $Y_I$ | $Y_{III}$ | $Y_I$ | $Y_{III}$ | $Y_I$ | $Y_{III}$ | $Y_I$ | $Y_{III}$ |
| | 0.00262 | 0 | 0.00203 | 0.00128 | 0.00162 | 0.00183 | 0.00122 | 0.00246 | 0 | 0.00332 |
| SCB | $\alpha = 0^\circ$ | | $\alpha = 15^\circ$ | | $\alpha = 30^\circ$ | | $\alpha = 45^\circ$ | | $\alpha = 60^\circ$ | |
| | $Y_I$ | $Y_{III}$ | $Y_I$ | $Y_{III}$ | $Y_I$ | $Y_{III}$ | $Y_I$ | $Y_{III}$ | $Y_I$ | $Y_{III}$ |
| | 0.17981 | 0 | 0.16964 | 0.02629 | 0.1380 | 0.04625 | 0.09865 | 0.05421 | 0.05247 | 0.04551 |
| TPB-IC | $\alpha = 0^\circ$ | | $\alpha = 15^\circ$ | | $\alpha = 30^\circ$ | | $\alpha = 45^\circ$ | | $\alpha = 60^\circ$ | |
| | $Y_I$ | $Y_{II}$ | $Y_I$ | $Y_{III}$ | $Y_I$ | $Y_{III}$ | $Y_I$ | $Y_{III}$ | $Y_I$ | $Y_{III}$ |
| | 0.05629 | 0 | 0.05288 | 0.00835 | 0.04417 | 0.01462 | 0.03125 | 0.01716 | 0.01671 | 0.01477 |
| SENB | $\alpha = 0^\circ$ | | $\alpha = 15^\circ$ | | $\alpha = 30^\circ$ | | $\alpha = 45^\circ$ | | $\alpha = 60^\circ$ | |
| | $Y_I$ | $Y_{III}$ | $Y_I$ | $Y_{III}$ | $Y_I$ | $Y_{III}$ | $Y_I$ | $Y_{III}$ | $Y_I$ | $Y_{III}$ |
| | 0.05629 | 0 | 0.05312 | 0.00783 | 0.04578 | 0.01268 | 0.03443 | 0.01703 | 0.01939 | 0.01429 |
| ATPB | $l = 0$ mm | | $l = 10$ mm | | $l = 20$ mm | | $l = 25$ mm | | | |
| | $Y_I$ | $Y_{III}$ | $Y_I$ | $Y_{III}$ | $Y_I$ | $Y_{III}$ | $Y_I$ | $Y_{III}$ | | |
| | 0.04731 | 0 | 0.04227 | 0.01199 | 0.02941 | 0.01294 | 0.02222 | 0.01184 | | |

The ENDC and DNDC specimens made of rock were positioned between two flat rigid plates under compression and tested using a universal testing machine with different crack inclination angles. The other specimens were subjected to 3-point bending with different combinations of modes I and III (as shown in **Fig. 5**). All the specimens were loaded monotonically with a constant displacement rate of 1 mm/min. The typical load-displacement responses of the specimens under mode-I loading are shown in **Fig. 6**. The initial nonlinearity in the load-displacement curves observed for some of the tested specimens was due to incomplete contact of the disc-shaped specimens with the loading roller at the start of the test. After forming a complete contact, the curves were linearized up to the maximum load corresponding to the initiation of failure in the tested specimens. The fracture toughness values of the specimens were determined by considering the maximum load achieved for the fracture tests using Eqs. (1– 6) and the geometrical factors provided in **Table 1** and **Table 2**.

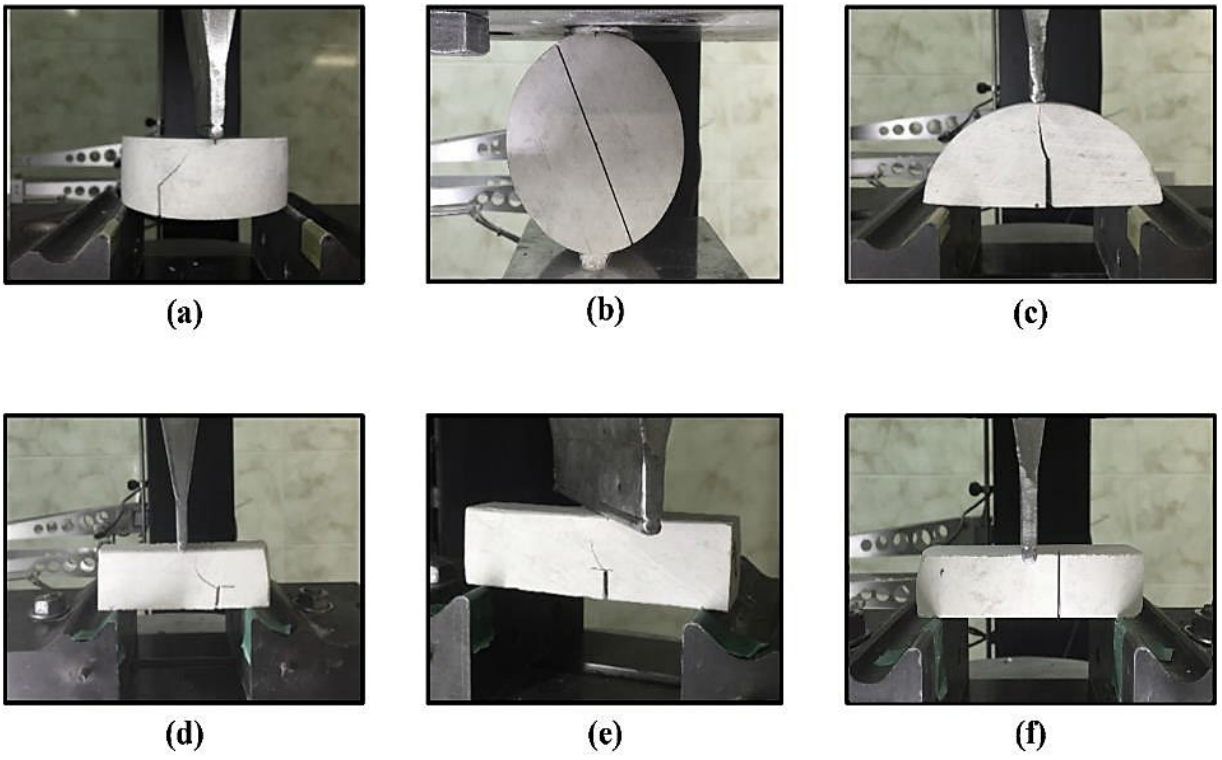


**Fig. 5.** Test setup for testing the specimens under opening-tearing mixed-mode loading; (a) ENDB, (b) ENDC and DNDC, (c) SCB, (d) TPB-IC, (e) SENB (e), and (f) ATPB.

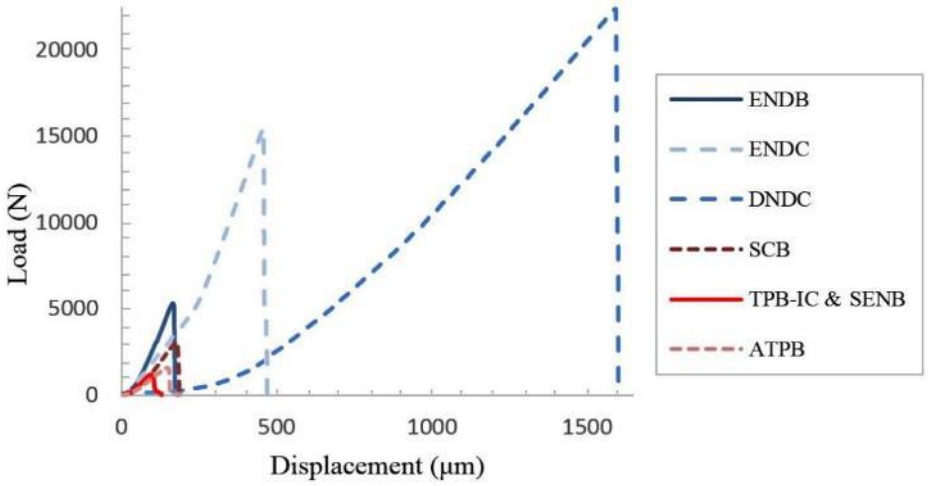


**Fig. 6.** Typical load-displacement curves obtained for different specimens under pure mode-I condition.

According to **Fig. 6**, the disc-shape specimens loaded between two parallel plates under compression (i.e. ENDC and DNDC) had the highest peak load levels under pure mode I compared to the other specimens that were loaded under 3-point bending. The highest and lowest peak loads under pure mode-I loading were obtained for the DNDC and TPB-IC or SENB specimens with the values of 22.5 and 1.1 kN, respectively. **Fig. 7(a)** shows the average fracture toughness variations in the form of $K_{\mathrm{IIIc}}$ against $K_{\mathrm{Ic}}$ curves for different specimens under mixed-mode I/III conditions. Moreover, **Fig. 7(b)** represents the mixed-mode fracture data in the form of the normalized effective fracture toughness ($K_{\mathrm{eff}}/K_{\mathrm{Ic}}$) versus the mode mixity parameter ($M_{\mathrm{e}}$). $K_{\mathrm{eff}}$ is defined as Eq. (8).

$$K_{\mathrm{eff}} = \sqrt{K_{\mathrm{I}}^2 + K_{\mathrm{III}}^2} \tag{8}$$

The scatter of the experimental results was in an acceptable range of 6-11% for the tested brittle rock material, demonstrating the consistency and repeatability of the tests. The results showed different trends in the fracture behaviors of the specimens with different geometries under mixed-mode I/III loading. Fig. 7(a) clearly shows the influence of specimen geometry and loading conditions on the fracture toughness of the tested rock material. As shown in Fig. 7(a), the pure opening mode fracture toughness values were determined from different specimen geometries scattered in a relatively narrow band with a maximum difference of 25%. This can also be seen in Fig. 7(b), in which the normalized effective fracture toughness versus the mode mixity parameter is depicted. The correlation between the fracture toughness values of different specimen geometries continued up to around the mode mixity of 0.65. However, by moving towards the tearing mode, the fracture toughness of different specimen geometries diverged. As can be seen in Fig. 7b, the normalized effective critical stress intensity factor of the TPB-IC, SENB, ATPB, and SCB specimens initially increased by moving towards pure mode III and then decreased. The normalized effective critical stress intensity factor of the ENDB specimen until the mode mixity of 0.4 remained almost constant and then decreased until $M_{\mathrm{e}}^{13}$=0. The variation trends of the normalized effective SIFs for the ENDC and DNDC specimens continuously increased when moving from opening mode to tearing mode. Comparing the effective fracture toughness variations of all the specimens tested in this study revealed that the highest value of the effective fracture toughness was obtained for the DNDC specimen under pure mode-III condition, while the lowest value was obtained for the TPB-IC specimen at $M_{\mathrm{e}}^{13}$=0.54. Other researchers (e.g. Aliha et al., 2017; Aliha et al., 2012; Chao et al., 2001; Muñoz-Ibáñez et al., 2021; Shahryari et al., 2021) showed that the mode-I fracture toughness values obtained from different specimens were depended on the loading condition and specimen geometry. This dependency was attributed to the different values of *T*-stress in different specimens. Similarly, the current study showed the dependency of the fracture resistance of different specimens on the specimen geometry under tension-tear loading. According to the *T*-stress and fracture toughness results, the *T*-stress values obtained for different geometries and loading conditions were different even though the mode mixity and the material were the same. In addition, a positive *T*-stress in the tested specimens increased the specimen's mixed-mode I/III fracture toughness. This trend was consistent with the maximum normal strain criterion (Aliha et al., 2012, 2017b, 2018; Liu & Chao, 2003; Muñoz-Ibáñez et al., 2021), where the higher negative *T*-stress resulted in a smaller $K_{\mathrm{Ic}}$ value. **Fig. 8** compares the fracture toughness values obtained for the pure opening and tearing modes from the specimens that covered pure modes.

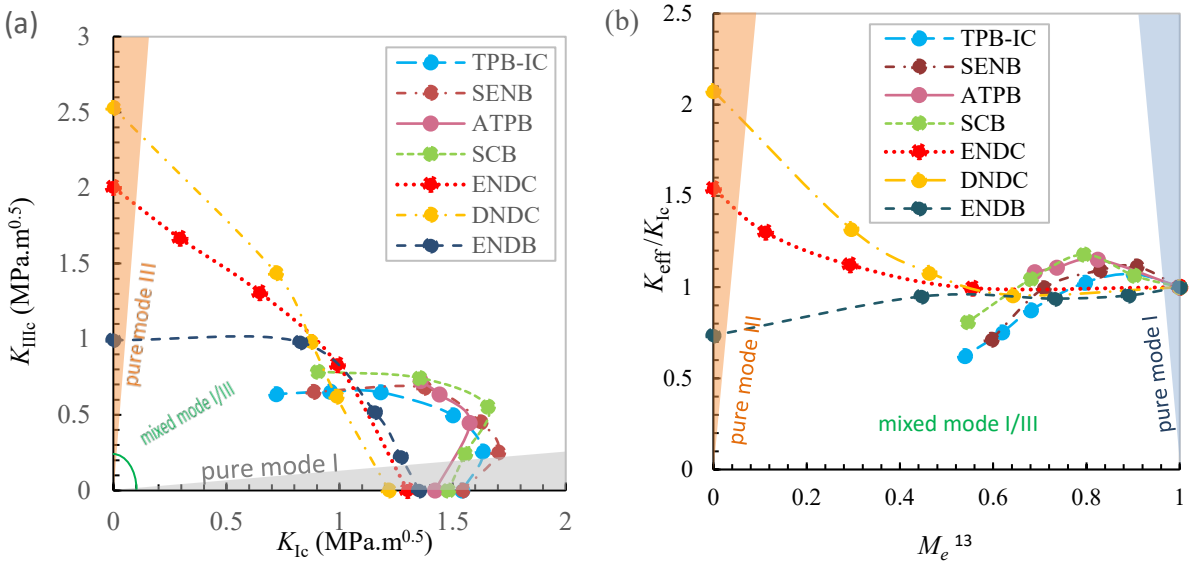


**Fig. 7.** (a) $K_{IIIc}$ against $K_{Ic}$ curves, and (b) $K_{eff}$/ $K_{Ic}$ against $M_e^{13}$ curves.

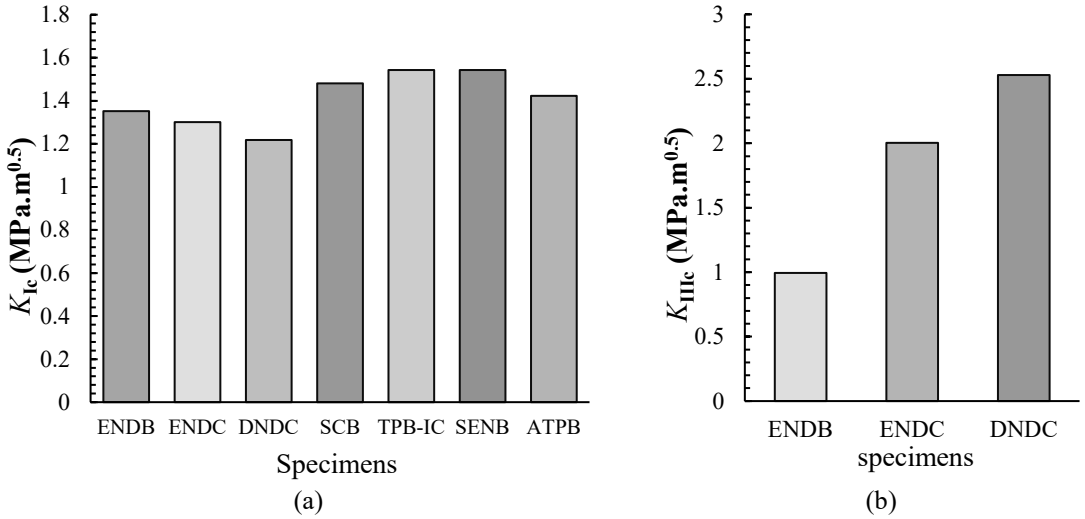


**Fig. 8.** Comparison between the fracture toughness values of (a) pure opening mode and (b) pure tearing mode.

As shown in **Fig. 8**, only the ENDB, ENDC, and DNDC specimens can cover pure mode III, and among the specimens that can cover pure mode III, the DNDC specimen provided the highest $K_{IIIc}$ value followed by the ENDC and ENDB samples. Moreover, it is observed that the highest fracture toughness obtained for pure opening mode was related to the TPB-IC and SENB specimens. The DNDC specimen had the lowest opening-mode fracture toughness. **Fig. 9** compares the fracture surfaces observed for the tested specimens. As it was expected, the specimens under pure opening mode had flat and smooth surfaces, while by shifting towards tearing mode, more complex fracture patterns were observed.

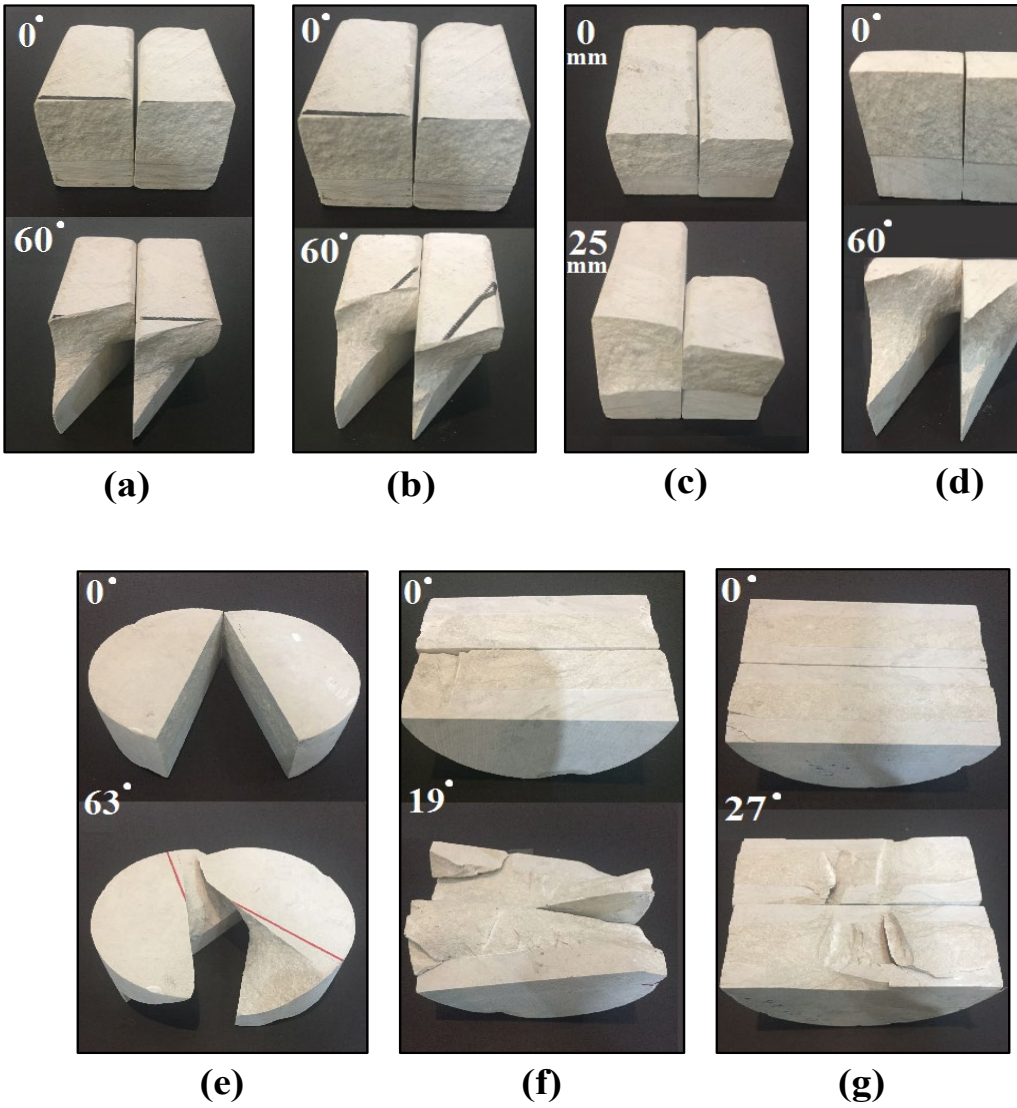


**Fig. 9.** Fracture surfaces observed for the specimens with different geometries under mixed mode I/III; a) TPB-IC, b) SENB, c) ATPB, d) SCB, e) ENDB, f) ENDC, g) DNDC.

The fracture surfaces pertinent to pure opening and tearing loading conditions for the ENDB, ENDC, and DNDC specimens, which could cover pure tearing mode, are shown in **Fig. 9**. For the other specimens, the fracture surfaces for the pure mode I and the minimum $M_e$[13] (the highest contribution of mode III) that could be achieved are shown in **Fig. 9**. As seen in Fig. 9, under the influence of tearing mode, the crack front tended to rotate and created some segmentation patterns. For the DNDC and ENDC specimens that had a large crack front, more wrinkles are observable in the opening-tearing mixed-mode fracture surfaces. This phenomenon can be observed in the fracture surfaces of the ENDC sample under opening-tearing mixed-mode and pure tearing conditions. The crack rotation and segmentation phenomena due to the tearing deformation have been explored through both experimental and theoretical approaches in the literature (Cambonie et al., 2019; Lazarus et al., 2001; Pham & Ravi-Chandar, 2016). As depicted in **Fig. 9**, for the ENDB specimen, the fracture trajectory transitioned from a straight and symmetric path (in a pure opening mode) to an anti-symmetric twisted trajectory (in a pure tearing mode). Moreover, the SCB, TPB-IC and SENB specimens also experienced some twisting in their fracture surfaces when tested under mixed mode I/III.

## 5. Conclusions

The influence of geometry and loading conditions on the opening-tearing mixed-mode fracture behavior of rock materials were investigated using seven different specimens, including the ENDB, ENDC, DNDC, SCB, TPB-IC, SENB, and ATPB specimens. The scatter of the fracture toughness experimental results was in the acceptable range of 6-11% for the tested marble rock samples, which showed the reliability and reproducibility of the tests. The results revealed different trends in the fracture behaviors of the samples with different geometries under I/III mixed mode loading. The normalized effective critical stress intensity factors (SIFs) of the TPB-IC, SENB, ATPB, and SCB samples initially increased by moving towards pure mode III and then decreased. The trend of changes in normalized effective SIFs for the ENDC and DNDC specimens was continuously increased when moving from opening to tearing mode. Comparing the effective fracture toughness changes of

all samples tested in this study showed that the highest value of effective fracture toughness was obtained for the DNDC specimen at pure mode III condition, while the lowest value was found for the TPB-IC specimen. The present study showed the dependency of the fracture toughness of different samples on the geometry of the sample under tensile-tear mixed mode loading. The consistency between the effective fracture toughness values obtained from different specimen geometries in the dominant mode-I region was relatively acceptable. However, as the specimens moved towards tearing mode, fracture toughness values diverged. Among the studied geometries, the TPB-IC and SENB specimens had the highest fracture toughness values in pure opening mode, while the DNDC specimen had the lowest value. Among the three specimens that could cover pure tearing mode (ENDB, ENDC, and DNDC), the DNDC specimen had the highest mode-III fracture toughness value, followed by the ENDC and ENDB specimens. The investigation of *T*-stress for different geometries and loading conditions revealed that although the material and mode mixity were the same in different specimen geometries, the *T*-stress values differed. It was also found that a positive *T*-stress value increased the fracture toughness of mixed-mode I/III, while a negative *T*-stress value decreased it. Furthermore, investigating the fracture surfaces of different specimens showed that the ENDC and DNDC specimens had more wrinkles on their fracture surfaces under opening-tearing mixed-mode conditions compared to the ENDB, SCB, TPB-IC, SENB, and ATPB specimens.

## References


Abdollahipour, A., Fatehi Marji, M., Yarahmadi Bafghi, A., & Gholamnejad, J. (2016). DEM simulation of confining pressure effects on crack opening displacement in hydraulic fracturing. *International Journal of Mining Science and Technology, 26*(4), 557-561. https://doi.org/https://doi.org/10.1016/j.ijmst.2016.05.004

Ahmadi, M., Shafabakhsh, G. A., Di Mascio, P., & Hassani, A. (2021). Failure behavior of functionally graded roller compacted concrete pavement under mode I and III fracture. *Construction and Building Materials, 307*, 124942.

Ahmadi-Moghadam, B., Taheri, F. (2013). An effective means for evaluating mixed-mode I/III stress intensity factors using single-edge notch beam specimen. *The Journal of Strain Analysis for Engineering Design, 48*(4), 245-257. doi:10.1177/0309324713480767

Aliha, M. R. M., & Ayatollahi, M. R. (2014). Rock fracture toughness study using cracked chevron notched Brazilian disc specimen under pure modes I and II loading – A statistical approach. *Theoretical and Applied Fracture Mechanics, 69*, 17-25. https://doi.org/https://doi.org/10.1016/j.tafmec.2013.11.008

Aliha, M. R. M., & Bahmani, A. (2017). Rock Fracture Toughness Study Under Mixed Mode I/III Loading. *Rock Mechanics and Rock Engineering, 50*(7), 1739-1751. https://doi.org/10.1007/s00603-017-1201-7

Aliha, M. R. M., Ayatollahi, M., Smith, D., & Pavier, M. (2010). Geometry and size effects on fracture trajectory in a limestone rock under mixed mode loading. *Engineering Fracture Mechanics, 77*(11), 2200-2212.

Aliha, M. R. M., G. Kouchaki, H., & Jafari Haghighatpour, P. (2023). Designing a simple and suitable laboratory test specimen for investigating the general mixed mode I/II/III fracture problem. *Materials & Design, 236,* 112477. https://doi.org/https://doi.org/10.1016/j.matdes.2023.112477

Aliha, M. R. M., Mahdavi, E., & Ayatollahi, M. R. (2017a). The Influence of Specimen Type on Tensile Fracture Toughness of Rock Materials. *Pure and Applied Geophysics, 174*(3), 1237-1253. https://doi.org/10.1007/s00024-016-1458-x

Aliha, M. R. M., Berto, F., Bahmani, A., & Gallo, P. (2017b). Mixed mode I/II fracture investigation of Perspex based on the averaged strain energy density criterion. *Physical Mesomechanics, 20*(2), 149-156. https://doi.org/10.1134/S1029959917020059.

Aliha, M. R. M., Sarbijan, M., & Bahmani, A. (2017c). Fracture toughness determination of modified HMA mixtures with two novel disc shape configurations. *Construction and Building Materials, 155*, 789-799.

Aliha, M. R. M., Mahdavi, E., & Ayatollahi, M. R. (2018). Statistical Analysis of Rock Fracture Toughness Data Obtained from Different Chevron Notched and Straight Cracked Mode I Specimens. *Rock Mechanics and Rock Engineering, 51*(7), 2095-2114. https://doi.org/10.1007/s00603-018-1454-9

Aliha, M. R. M., Sistaninia, M., Smith, D. J., Pavier, M. J., & Ayatollahi, M. R. (2012). Geometry effects and statistical analysis of mode I fracture in guiting limestone. *International Journal of Rock Mechanics and Mining Sciences, 51*, 128-135. https://doi.org/https://doi.org/10.1016/j.ijrmms.2012.01.017

Aliha, M. R. M., & Ayatollahi, M. (2010). Geometry effects on fracture behaviour of polymethyl methacrylate. *Materials Science and Engineering: A, 527*(3), 526-530.

Aliha, M. R. M., Bahmani, A., & Akhondi, S. (2015). Numerical analysis of a new mixed mode I/III fracture test specimen. *Engineering Fracture Mechanics, 134*, 95-110.

Aliha, M. R. M., Ghesmati Kucheki, H., & Asadi, M. M. (2021). On the use of different diametral compression cracked disc shape specimens for introducing mode III deformation. *Fatigue & Fracture of Engineering Materials & Structures, 44*(11), 3135-3151.

Aliha, M. R. M., Karimi, H., & Ghoreishi, S. (2022). Design and validation of simple bend beam specimen for covering the full range of I+ II fracture modes. *European Journal of Mechanics-A/Solids, 91*, 104425.

Awaji, H., & Sato, S. (1978). Combined mode fracture toughness measurement by the disk test.

Ayatollahi, M. R., & Saboori, B. (2015). A new fixture for fracture tests under mixed mode I/III loading. *European Journal of Mechanics - A/Solids, 51*, 67-76. https://doi.org/https://doi.org/10.1016/j.euromechsol.2014.09.012

Ayatollahi, M. R., Pavier, M. J., & Smith, D. J. (1998). Determination of T-stress from finite element analysis for mode I and mixed mode I/II loading. *International Journal of Fracture, 91*(3), 283-298. https://doi.org/10.1023/A:1007581125618

Ayatollahi, M. R., & Aliha, M. R. M., (2008). On the use of Brazilian disc specimen for calculating mixed mode I–II fracture toughness of rock materials. *Engineering Fracture Mechanics, 75*(16), 4631-4641.

Ayatollahi, M. R., Aliha, M. R. M., & Saghafi, H. (2011). An improved semi-circular bend specimen for investigating mixed mode brittle fracture. *Engineering Fracture Mechanics, 78*(1), 110-123.

Bahmani, A., & Nemati, S. (2021). Fracture resistance of railway ballast rock under tensile and tear loads. *Engineering Solid Mechanics, 9*(3), 271-280.

Bahmani, A., Farahmand, F., Ataei, F., & Aliha, M. R. M. (2019). Mixed mode I/III fracture parameters for edge-notched diametrically compressed disc specimen. *Material Design & Processing Communications, 1*(6), e86. https://doi.org/https://doi.org/10.1002/mdp2.86

Bahmani, A., Farahmand, F., Janbaz, M. R., Darbandi, A. H., Ghesmati-Kucheki, H., & Aliha, M. R. M. (2021). On the comparison of two mixed-mode I+ III fracture test specimens. *Engineering Fracture Mechanics, 241,* 107434.

Bakhshizadeh, M., Hartford, S., Karimi, H. R., & Aliha, M. R. M. (2024). Effect of support friction on pure mode I, II, and III fracture toughness of cement concrete tested with edge-notched disc bend specimen. *Theoretical and Applied Fracture Mechanics, 129*, 104247. https://doi.org/https://doi.org/10.1016/j.tafmec.2023.104247

Bazoobandi, P., Mousavi, S. R., Karimi, F., Karimi, H. R., Ghasri, M., & Aliha, M. (2024). Cracking resistance of crumb rubber modified green asphalt mixtures, using calcium carbonate nanoparticles and two by-product wax-based warm mix additives. *Construction and Building Materials, 424*, 135848. https://doi.org/10.1016/j.conbuildmat.2024.135848

Bidadi, J., Aliha, M. R. M., & Akbardoost, J. (2022). Development of maximum tangential strain (MTSN) criterion for prediction of mixed-mode I/III brittle fracture. *International Journal of Solids and Structures, 256*, 111979.

Cambonie, T., Klinger, Y., & Lazarus, V. (2019). Similarities between mode III crack growth patterns and strike-slip faults. *Philosophical Transactions of the Royal Society A: Mathematical, Physical and Engineering Sciences, 377*(2136), 20170392. https://doi.org/doi:10.1098/rsta.2017.0392

Cao, P., Zhou, T., & Zhu, J. (2023). Strain rate effect on mixed mode I/II fracture toughness of sandstone and its micromechanism. *International Journal of Rock Mechanics and Mining Sciences, 165*, 105379. https://doi.org/https://doi.org/10.1016/j.ijrmms.2023.105379

Chao, Y. J., Liu, S., & Broviak, B. J. (2001). Brittle fracture: Variation of fracture toughness with constraint and crack curving under mode I conditions. *Experimental Mechanics, 41*(3), 232-241. https://doi.org/10.1007/BF02323139

Cui, L., & McAdie, A. (2023). Experimental study on evolutive fracture behavior and properties of sulfate-rich fiber-reinforced cemented paste backfill under pure mode-I, mode-II, and mode-III loadings. *International Journal of Rock Mechanics and Mining Sciences, 169,* 105434.

Fan, Y., Zhu, Z., Zhao, Y., Zhou, L., Qiu, H., & Niu, C. (2021). Analytical solution of T-stresses for an inclined crack in compression. *International Journal of Rock Mechanics and Mining Sciences, 138,* 104433. https://doi.org/https://doi.org/10.1016/j.ijrmms.2020.104433

Gan, Z., Hua, W., Wang, A., Fan, Z., Huang, J., Dong, S., & Wu, H. (2024). Experimental investigation on mixed mode I-III fracture behaviors and degradation mechanism of sandstone under thermal-chemical stimulation. *Theoretical and Applied Fracture Mechanics, 129,* 104188.

Gan, Z., Pan, X., Tang, H., Huang, J., Dong, S., & Hua, W. (2021). Experimental investigation on mixed mode I-III fracture characteristics of sandstone corroded by periodic acid solution. *Theoretical and Applied Fracture Mechanics, 114*, 103034.

Gao, M., Zhang, C., & Oh, J. (2023). Assessments of the effects of various fracture surface morphology on single fracture flow: A review. *International Journal of Mining Science and Technology, 33*(1), 1-29. https://doi.org/https://doi.org/10.1016/j.ijmst.2022.07.005

Guan, J., Zhang, Y., Meng, J., Yao, X., Li, L., & He, S. (2022). A simple method for determining independent fracture toughness and tensile strength of rock. *International Journal of Mining Science and Technology, 32*(4), 707-726. https://doi.org/https://doi.org/10.1016/j.ijmst.2022.05.004

Hasanpour, R., & Choupani, N. (2009). Rock fracture characterization using the modified Arcan test specimen. *International Journal of Rock Mechanics and Mining Sciences, 46*(2), 346-354.

Hoseini, S. O., Mousavi, S. R., Sohrabi, M. R., & Ghasemi, M. (2023). Using beam and ENDB specimens to evaluate fracture characteristics of wavy steel fiber-reinforced self-compacting concrete containing different coarse aggregate volumes. *Fatigue & Fracture of Engineering Materials & Structures, 46*(5), 1669-1686. https://doi.org/https://doi.org/10.1111/ffe.13942

Hoseini, S. O., Sohrabi, M. R., Mousavi, S. R., & Ghasemi, M. (2022). Effects of coarse aggregate and wavy steel fiber volumes on the critical stress intensity factors of modes I and III cracks in self-compacting concrete using ENDB specimens. *Theoretical and Applied Fracture Mechanics, 121*, 103421. https://doi.org/https://doi.org/10.1016/j.tafmec.2022.103421

Hoseini, S. O., Sohrabi, M. R., Mousavi, S. R., Ghasemi, M., & Aliha, M. R. M. (2024). Comparing Different Procedures for Calculating Flexural Cracking Toughness Using Edge-Notched Disc Bend Specimen Under Modes I and III. *Fatigue & Fracture of Engineering Materials & Structures*. https://doi.org/10.1111/ffe.14530

Karimi, H. R., Aliha, M. R. M., Khedri, E., Mousavi, A., Salehi, S. M., Haghighatpour, P. J., & Ebneabbasi, P. (2023). Strength and cracking resistance of concrete containing different percentages and sizes of recycled tire rubber granules. *Journal of Building Engineering, 67,* 106033. https://doi.org/https://doi.org/10.1016/j.jobe.2023.106033

Karimi, H. r., Khedri, E., Aliha, M. R. M., & Mousavi, A. (2022). A comprehensive study on ring shape specimens under compressive and tensile loadings for covering the full range of I+II fracture modes of gypsum material. *International Journal of Rock Mechanics and Mining Sciences, 160*, 105265. https://doi.org/https://doi.org/10.1016/j.ijrmms.2022.105265

Karimi, H. R., Khedri, E., Mousavi, A., Taherifar, A., Abdoli, Z., & Mohamadi, R. (2024). Mode I/II cracking behavior of additively manufactured interpenetrating phase composites (IPC), an experimental and theoretical study. *Theoretical and Applied Fracture Mechanics, 131*, 104396. https://doi.org/10.1016/j.tafmec.2024.104396

Khanghahi, S. H., Hadidi, M. R., & Mohammadi, Y. (2024). Laboratory Investigations on Fracture Toughness of Self-compacting Concrete Containing Recycled Materials. *Jordan Journal of Civil Engineering, 18*(2).

Lazarus, V., Leblond, J.-B., & Mouchrif, S.-E. (2001). Crack front rotation and segmentation in mixed mode I+III or I+II+III. Part II: Comparison with experiments. *Journal of the Mechanics and Physics of Solids, 49*(7), 1421-1443. https://doi.org/https://doi.org/10.1016/S0022-5096(01)00008-4

Li, C., Yang, D., Xie, H., Ren, L., & Wang, J. (2023). Size effect of fracture characteristics for anisotropic quasi-brittle geomaterials. *International Journal of Mining Science and Technology, 33*(2), 201-213. https://doi.org/https://doi.org/10.1016/j.ijmst.2022.11.004

Liu, S., & Chao, Y. J. (2003). Variation of fracture toughness with constraint. *International Journal of Fracture, 124*(3), 113-117. https://doi.org/10.1023/B:FRAC.0000018230.97560.ae

Liu, Z., & Ma, C. (2023). Study on fracture behavior of layered limestone under mixed mode I/III loading. Theoretical and *Applied Fracture Mechanics, 128*, 104102.

Li-yun, L., Zhi-qiang, X., Ming-xiu, L., Yi, L., Chen, F., Tie-Wu, T., & Da-an, L. (2013). A experimental study of I-II-III mixed mode crack fracture of rock under different temperature *In 13th International Conference on Fracture*, Beijing, China

Maccagno, T., & Knott, J. (1989). The fracture behaviour of PMMA in mixed modes I and II. *Engineering Fracture Mechanics, 34*(1), 65-86.

Mahajan, R., & Ravi-Chandar, K. (1989). An experimental investigation of mixed-mode fracture. *International Journal of fracture, 41*(4), 235-252.

Marat-Mendes, R., & De Freitas, M. (2009). Characterisation of the edge crack torsion (ECT) test for the measurement of the mode III interlaminar fracture toughness. *Engineering Fracture Mechanics, 76*(18), 2799–2809. https://doi.org/10.1016/j.engfracmech.2009.06.016

Mirsayar, M.M., Aliha, M.R.M., & Samaei, A.T. (2014). On fracture initiation angle near bi-material notches- Effects of first non-singular stress term. *Engineering Fracture Mechanics, 119*, 124-131.

Mousavi, S. R., Afshoon, I., Bayatpour, M. A., TQ, A. D., & Miri, M. (2021). Effect of waste glass and curing aging on fracture toughness of self-compacting mortars using ENDB specimen. *Construction and Building Materials, 282*, 122711.

Mousavi, S., Ghasemi, M., & Dehghani, M. (2024). Investigating the fracture toughness of the self compacting concrete using ENDB samples by changing the aggregate size and percent of steel fiber. *Engineering Solid Mechanics, 12*(1), 17-26.

Muñoz-Ibáñez, A., Delgado-Martín, J., & Juncosa-Rivera, R. (2021). Size effect and other effects on mode I fracture toughness using two testing methods. *International Journal of Rock Mechanics and Mining Sciences, 143*, 104785. https://doi.org/https://doi.org/10.1016/j.ijrmms.2021.104785

Najjar, S., Moghaddam, A. M., Sahaf, A., & Aliha, M. R. M. (2020). Low temperature fracture resistance of cement emulsified asphalt mortar under mixed mode I/III loading. *Theoretical and Applied Fracture Mechanics, 110*, 102800.

Najjar, S., Moghaddam, A. M., Sahaf, A., & Aliha, M. R. M. (2022). Aging effect on the mixed-mode (I/III) fracture toughness of cement emulsified asphalt composite: Experimental and statistical investigation. *Engineering Fracture Mechanics, 264*, 108292.

Pan, X., Huang, J., Gan, Z., Dong, S., & Hua, W. (2021). Analysis of Mixed-Mode I/II/III Fracture Toughness Based on a Three-Point Bending Sandstone Specimen with an Inclined Crack. *Applied Sciences, 11*(4), 1652.

Pham, K. H., & Ravi-Chandar, K. (2016). On the growth of cracks under mixed-mode I + III loading. *International Journal of Fracture, 199*(1), 105-134. https://doi.org/10.1007/s10704-016-0098-6

Pietras, D., Aliha, M. R. M., & Sadowski, T. (2021). Mode III fracture toughness testing and numerical modeling for aerated autoclaved concrete using notch cylinder specimen subjected to torsion. *Materials Today: Proceedings, 45*, 4326-4329.

Pietras, D., Aliha, M. R. M., Kucheki, H. G., & Sadowski, T. (2023). Tensile and tear-type fracture toughness of gypsum material: Direct and indirect testing methods. *Journal of Rock Mechanics and Geotechnical Engineering, 15*(7), 1777-1796. https://doi.org/https://doi.org/10.1016/j.jrmge.2022.11.016

Pirmohammad, S., & Bayat, A. (2016). Characterizing mixed mode I/III fracture toughness of asphalt concrete using asymmetric disc bend (ADB) specimen. *Construction and Building Materials, 120*, 571-580.

Pirmohammad, S., & Kiani, A. (2016). Study on fracture behavior of HMA mixtures under mixed mode I/III loading. *Engineering Fracture Mechanics, 153*, 80-90.

Pournoori, P., Davarpanah TQ, A., Rajaee, A., Ghodratnama, M., Abrishami, S., & Masoodi, A. R. (2024). Experimental exploration of fracture behavior (pure mode III) in eco-friendly steel fiber-reinforced self-compacting concrete with waste tempered glass as coarse aggregates. *Scientific Reports, 14*(1), 9043.

Qiu, J., Luo, L., Li, X., Li, D., Chen, Y., & Luo, Y. (2020). Numerical investigation on the tensile fracturing behavior of rock-shotcrete interface based on discrete element method. *International Journal of Mining Science and Technology, 30*(3), 293-301. https://doi.org/https://doi.org/10.1016/j.ijmst.2020.03.007

Raeisi, R., Rezaie, F., & Aliha, M. R. M. (2024). Mixed mode I/II and I/III fracture toughness investigation for preplaced aggregate concrete mixtures: Experimental study and theoretical prediction. *Fatigue & Fracture of Engineering Materials & Structures, 47*(8), 2873-2887.

Shabakhty, N., Karimi, H. R., & Bakhtiary, A. Y. (2024). Cementitious composites in aquatic environments, evaluation of fracture and mechanical behavior in long-term submerging in fresh and saltwater, and simulated splash zone conditions. *Case Studies in Construction Materials, 20*, e03035. https://doi.org/10.1016/j.cscm.2024.e03035

Shahryari, N., Keymanesh, M. R., & Aliha, M. R. M. (2021). Specimen type effect on measured low-temperature fracture toughness of asphalt concrete. *Fatigue & Fracture of Engineering Materials & Structures, 44*(2), 551-567. https://doi.org/https://doi.org/10.1111/ffe.13379

Shi, Z., Li, J., Ranjith, P. G., Wang, M., Lin, H., Han, D., & Li, K. (2024). Acoustic emission and fracture morphology characteristics of thermal-damage granite under mixed mode I/III loading. *Theoretical and Applied Fracture Mechanics*, 104524.

Shui, X., Zhou, L., Zhu, Z., Nie, F., Wang, H., & Zhang, H. (2024). Investigation of the fracture characteristics of mixed-mode I/III crack by using two kinds of sandstone specimens. *Engineering Fracture Mechanics, 310*, 110488.

Smith, D. J., Ayatollahi, M. R., & Pavier, M. J. (2001). The role of T-stress in brittle fracture for linear elastic materials under mixed-mode loading. *Fatigue & Fracture of Engineering Materials & Structures, 24*(2), 137-150. https://doi.org/https://doi.org/10.1046/j.1460-2695.2001.00377.x

Smith, D. J., Ayatollahi, M. R., & Pavier, M. J. (2006). On the consequences of T-stress in elastic brittle fracture. *Proceedings of the Royal Society A: Mathematical, Physical and Engineering Sciences, 462*(2072), 2415-2437. https://doi.org/doi:10.1098/rspa.2005.1639

Sreenath, S., Mohan, K. S. R., & Murali, G. (2022). Fracture toughness of reactive powder fibrous concrete composites under pure and mixed modes (I/III). *Buildings, 12*(5), 599.

Tang, W., Zhang, Y., Zhao, Y., Zheng, K., Wang, C., & Bi, J. (2024). Assessment of basalt fiber and gelling enhancement effects on mixed mode I/III fracture performance of the mortar composites. *Theoretical and Applied Fracture Mechanics, 130*, 104303.

Toshio, N., & Parks, D. M. (1992). Determination of elastic T-stress along three-dimensional crack fronts using an interaction integral. *International Journal of Solids and Structures, 29*, 1597-1611.

Wan, D., Wang, M., Zhu, Z., Wang, F., Zhou, L., Liu, R., Gao, W., Shu, Y., & Xiao, H. (2022). Coupled GIMP and CPDI material point method in modelling blast-induced three-dimensional rock fracture. *International Journal of Mining Science and Technology, 32*(5), 1097-1114. https://doi.org/https://doi.org/10.1016/j.ijmst.2022.08.012

Xeidakis, G., Samaras, I., Zacharopoulos, D., & Papakaliatakis, G. (1996). Crack growth in a mixed-mode loading on marble beams under three point bending. *International journal of fracture, 79*(2), 197-208.

Yang, Z., Yin, T., Zhuang, D., Wu, Y., Yin, J., & Chen, Y. (2022). Effect of temperature on mixed mode I/III fracture behavior of diorite: An experimental investigation. *Theoretical and Applied Fracture Mechanics, 122*, 103571.

Yao, W., Xu, Y., Wang, C., Xia, K., & Hokka, M. (2021). Dynamic Mode II fracture behavior of rocks under hydrostatic pressure using the short core in compression (SCC) method. *International Journal of Mining Science and Technology, 31*(5), 927-937. https://doi.org/https://doi.org/10.1016/j.ijmst.2021.08.001

Yu, H., & Kuna, M. (2021). Interaction integral method for computation of crack parameters K–T – A review. *Engineering Fracture Mechanics, 249*, 107722. https://doi.org/10.1016/j.engfracmech.2021.107722

Zarei, M., Abdi Kordani, A., & Zahedi, M. (2022). Evaluating the fracture behaviour of modified asphalt concrete composites (ACC) at low and intermediate temperatures using edge notched disc bend (ENDB) specimen. *Road Materials and Pavement Design, 23*(8), 1917-1941.

Zarei, M., Kordani, A. A., Zahedi, M., Akbarinia, F., & Khanjari, M. (2021). Evaluation of low and intermediate temperatures fracture indices for modified Warm mix asphalt (WMA) using edge notched disc bend (ENDB) specimen. *Theoretical and Applied Fracture Mechanics, 116,* 103137.

Zhang, J., Miao, X., Huang, Y., & Li, M. (2014). Fracture mechanics model of fully mechanized top coal caving of shallow coal seams and its application. *International Journal of Mining Science and Technology, 24*(3), 349-352. https://doi.org/https://doi.org/10.1016/j.ijmst.2014.03.011

Zhao, Y., Tang, W., Zhang, Y., Du, C., Li, Y., Wang, C., & Bi, J. (2024). Evaluating fracture resistance of basalt fiber reinforced mortar to mode I/III load using edge notched disc bend (ENDB) specimen: Insights from acoustic emission and morphological analysis. *Construction and Building Materials, 411*, 134421.

Zheng, J., Guo, J., Wang, J., Sun, H., Deng, J., & Lv, Q. (2022). A universal elliptical disc (UED) model to represent natural rock fractures. *International Journal of Mining Science and Technology, 32*(2), 261-270. https://doi.org/https://doi.org/10.1016/j.ijmst.2021.12.001